GeoHealth

RESEARCH ARTICLE
10.1029/2022GH000669

Key Points:

- A novel framework was proposed for healthy route planning with less $PM_{2.5}$ exposure
- Estimation models of fine scale on-road $PM_{2.5}$ have been proposed and validated
- A mobile application that provides healthy travel route planning has been developed

Supporting Information:

Supporting Information may be found in the online version of this article.

Correspondence to:

Z. Shi, W. Shi and A. Zhang,
shizhicheng@szu.edu.cn;
john.wz.shi@polyu.edu.hk;
april-anshu.zhang@polyu.edu.hk

Citation:

Tong, C., Shi, Z., Shi, W., & Zhang, A. (2022). Estimation of on-road $PM_{2.5}$ distributions by combining satellite top-of-atmosphere with microscale geographic predictors for healthy route planning. *GeoHealth*, *6*, e2022GH000669. https://doi.org/10.1029/2022GH000669

Received 7 JUN 2022
Accepted 1 SEP 2022

Estimation of On-Road $PM_{2.5}$ Distributions by Combining Satellite Top-of-Atmosphere With Microscale Geographic Predictors for Healthy Route Planning

Chengzhuo Tong[1], Zhicheng Shi[2], Wenzhong Shi[1], and Anshu Zhang[1]

[1]Otto Poon Charitable Foundation Smart Cities Research Institute and Department of Land Surveying and Geo-Informatics, The Hong Kong Polytechnic University, Hong Kong, China, [2]Research Institute for Smart Cities, School of Architecture and Urban Planning, Shenzhen University, Shenzhen, China

Abstract How to reduce the health risks for commuters, caused by air pollution such as $PM_{2.5}$ has always been an urgent issue needing to be solved. Proposed in this study, is a novel framework which enables greater avoidance of pollution and hence assists the provision of healthy travel. This framework is based on the estimation of on-road $PM_{2.5}$ throughout the whole city. First, the micro-scale $PM_{2.5}$ is predicted by land use regression (LUR) modeling enhanced by the use of the Landsat-8 top-of-atmosphere (TOA) data and microscale geographic predictors. In particular, the green view index (GVI) factor derived, the sky view factor, and the index-based built-up index, are incorporated within the TOA-LUR modeling. On-road $PM_{2.5}$ distributions are then mapped in high-spatial-resolution. The maps obtained can be used to find healthy travel routes with less $PM_{2.5}$. The proposed framework was applied in high-density Hong Kong by Landsat 8 images. External testing was based on mobile measurements. The results showed that the estimation performance of the proposed seasonal TOA-LUR Geographical and Temporal Weighted Regression models is at a high-level with an R^2 of 0.70–0.90. The newly introduced GVI index played an important role in these estimations. The $PM_{2.5}$ distribution maps at high-spatial-resolution were then used to develop an application providing Hong Kong residents with healthy route planning services. The proposed framework can, likewise, be applied in other cities to better ensure people's health when traveling, especially those in high-density cities.

Plain Language Summary Every year, exposure to outdoor air pollution has caused 7 million premature deaths and resulted in the loss of millions more healthy years of life. Therefore, it's critical to establish planning tools to support people's healthier and cleaner daily travel. By land use regression (LUR) modeling enhanced by the Landsat-8 top-of-atmosphere (TOA) data and microscale geographic predictors, the original framework proposed in this study provides an estimation and a mapping of on-road $PM_{2.5}$ at the fine scale, providing people with healthier travel choices. The estimation performance of the proposed seasonal TOA-LUR Geographical and Temporal Weighted Regression models achieved a high R^2 of 0.70–0.90. It may become a reference and guide for high-density cities, for smart travel planning and refined monitoring of air pollution in urban areas. It is hoped, therefore, that this study assists more people in urban areas to reduce their exposure to outdoor air pollution, both to protect their health, and assist in the construction of healthy cities, especially for the high-density city.

1. Introduction

In the latest handbook on sustainable urban mobility and spatial planning by United Nations (United Nations, 2020), a series of practical recommendations is outlined: (a) Active mobility is a core element of healthy cities in Mobility and Spatial Planning; (b) Both walking and cycling need to be supported not just in urban cores, but on a much larger scale; (c) Cities need to develop user-friendly applications that support healthy cycling and walking. In the current daily health travel, outdoor air pollution related to $PM_{2.5}$ has become one of the main sources of harm to people's health (Edwards et al., 2021). A recent global study published in the Bulletin of the World Health Organization estimates that 4.2 million premature deaths worldwide were caused by $PM_{2.5}$ each year (Nazarenko et al., 2021). This included more than 1 million deaths in China, more than 500,000 deaths in India, nearly 200,000 in Europe, and more than 50,000 in the United States (Nazarenko et al., 2021). Most of these deaths occurred during outdoor activities. Thus, given the current "new-found" health awareness, on how to estimate on-road $PM_{2.5}$ at a high-spatial-resolution and consequently heighten the ability to enable

healthy travel, route planning has become one of the urgent issues relating to urban smart active mobility, especially for high-density cities with serious air pollution.

However, due to the high maintenance costs of traditional ground monitoring systems (J. Li et al., 2020), spatial coverage to reflect microscale detailed on-road $PM_{2.5}$ variations is lacking (Lu et al., 2021). Therefore, it is crucial to accurately estimate micro-scale $PM_{2.5}$ distributions at high spatial resolution through multi-source data imagery and analysis.

Estimating $PM_{2.5}$ based on satellite remote sensing can make up for the lack of ground observation sites (T. Li et al., 2020). Remote sensing observations can provide longer-term observational data, with global coverage, higher spatial resolution, and low cost, a matter more conducive to the study of the spread of $PM_{2.5}$ (Li et al., 2021; Shogrkhodaei et al., 2021; D. Zhang et al., 2021). In the early stage, based on the aerosol optical depth (AOD) data retrieved from remote sensing data, and $PM_{2.5}$ measurements at ground stations, the $PM_{2.5}$ concentration value within or between regions can be effectively estimated by establishing a linear regression model between AOD and $PM_{2.5}$ (Braggio et al., 2021; Meng et al., 2021). By incorporating the meteorological factors, the multiple linear regression (MLR) model was then further used to more accurately represent the relationship between AOD and $PM_{2.5}$ (Ghahremanloo et al., 2021; X.Xu et al., 2021). Furthermore, the spatiotemporal geographic weighting models could estimate the $PM_{2.5}$ concentration (W. Chen et al., 2020; Xue et al., 2020; Y. Zhang et al., 2020). However, because the spatial scale is limited by the resolution of remote sensing images, for example, the resolution of the most commonly used MODIS AOD products is greater than or equal to 1 km (Wang et al., 2021; Wei et al., 2021), hence it cannot effectively identify pollution hotspots and accurately reflect spatial variation in urban areas.

Some studies recently, explored, has been the retrieval of ground $PM_{2.5}$ directly from the top-of-atmosphere (TOA) reflectance data of MODIS, while omitting the intermediate process of avoiding AOD retrieval (J. Liu et al., 2019; Yan et al., 2020; Yang et al., 2020). A multispectral empirical model has also, been proposed to estimate the concentration of $PM_{2.5}$ using Landsat 8 OLI and by taking into account the corresponding meteorological parameters (Mishra et al., 2021). The results have shown a high degree of accuracy. However, the microscale environmental factors such as urban spatial morphology, and vegetation distribution in the urban canopy, both of which are more essential in impacting $PM_{2.5}$ distribution in a high-density urban environment, have not been considered in the existing TOA-$PM_{2.5}$ studies. Thus currently, most existing TOA-$PM_{2.5}$ studies cannot reflect the spatial variability of microscale $PM_{2.5}$.

Previously, a framework using mobile measurement, Google Street View (GSV) data, Landsat data, and other data, has been proposed to estimate $PM_{2.5}$ concentration by land-use regression (LUR) models in the microscale urban environment (Tong et al., 2021). It has greatly improved the modeling and mapping of $PM_{2.5}$ at the microscale. However, due to the limitation of the application range of mobile measurement instruments, this framework cannot be applied to the entirety of an urban area.

To overcome the above limitations, the aim of this study is to provide a fine-scale estimation of the spatiotemporal variation of $PM_{2.5}$ in the high-density city environment for assisting healthy route planning with less $PM_{2.5}$. An improved framework has been proposed based on the following steps: (a) using the Landsat-8 TOA data to enhance LUR modeling to retrieve micro-scale $PM_{2.5}$ on roads. In this process, observation angle data of Landsat-8 satellite, $PM_{2.5}$ data of ground stations, urban environmental data (e.g., GSV images, OpenStreet-Map (OSM) data, and land use data), and meteorological data will be integrated into the LUR modeling (Gong et al., 2018; Kang et al., 2020; Y. Liu et al., 2021). In particular, the green view index (GVI) factor of green vegetation coverage of the urban canopy, the sky view factor (SVF) related to the three-dimensional environment of urban buildings, and the index-based built-up index (IBI), related to urban impervious surfaces, are considered in the modeling. (b) On-road $PM_{2.5}$ distributions of the whole city are further mapped at high-spatial-resolution. (c) Result maps of on-road $PM_{2.5}$ estimation are able to be used in the digital application for calculating the healthy travel route with less $PM_{2.5}$, to support the planning result.

Hong Kong, a representative of high-density cities, was selected as the study area, in which to apply the improved framework. From 2019 to 2021, more than 1,200 people died each year in Hong Kong due to outdoor air pollution such as $PM_{2.5}$ (The University of Hong Kong, 2022). Therefore, how to reduce people's $PM_{2.5}$ exposure and consequently better ensure their health during mobility is an urgent need in high-density cities such as Hong Kong. In this study, the fine-scale spatiotemporal distribution of ground-level $PM_{2.5}$ over Hong Kong was estimated by the TOA-LUR modeling with the Landsat-8 TOA data for the period of 2014–2021, GSV, OSM data, and other

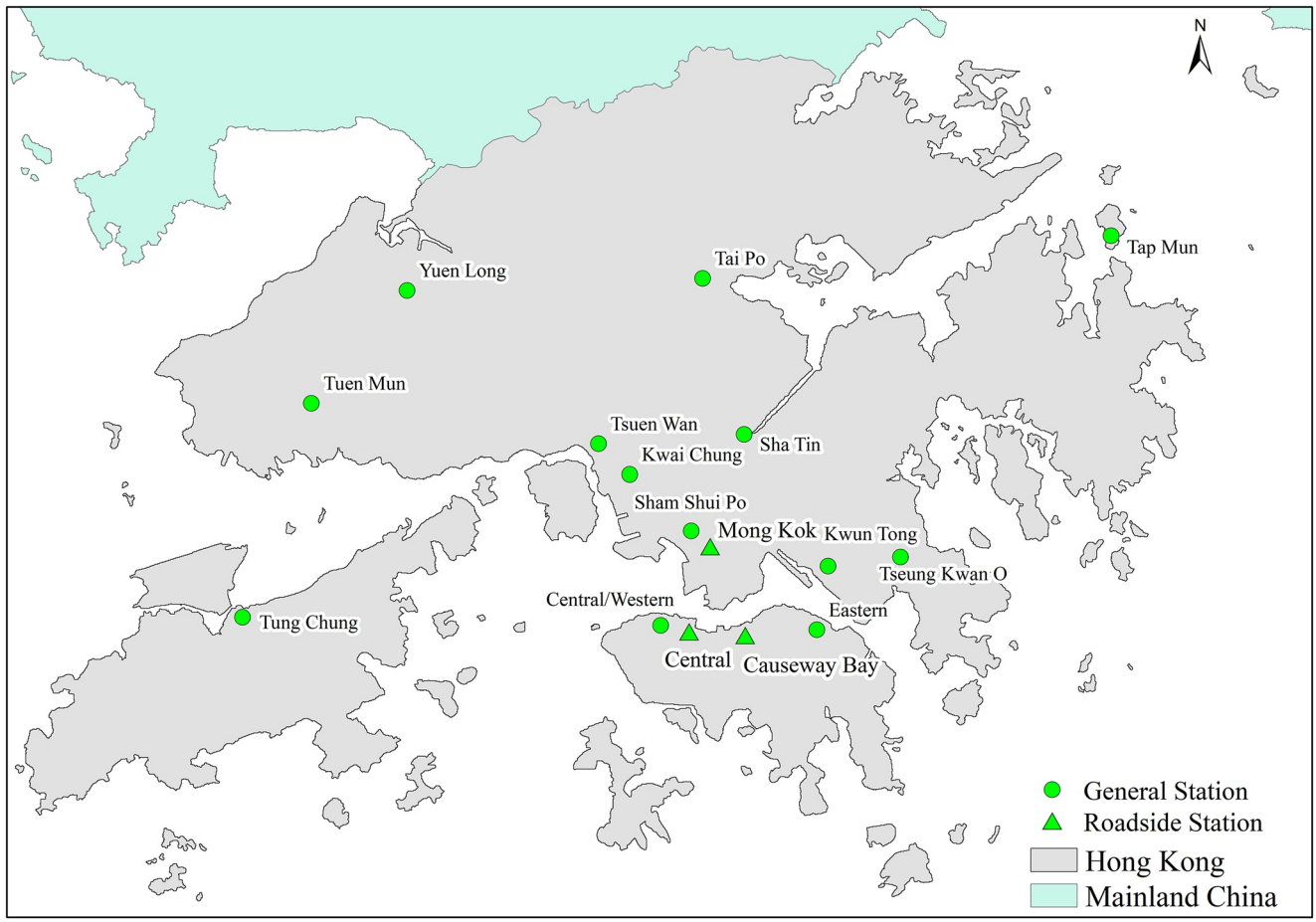

Figure 1. The locations of 16 air quality monitoring stations in Hong Kong.

multi-source geographic predictor data. Handheld $PM_{2.5}$ measuring instruments—Airbeam2 were further used to conduct the external test with the estimation results on the selected dates of the satellite transit during the whole of 2019 and 2021. Aided by the obtained on-road $PM_{2.5}$ distribution maps at high-spatial-resolution, a related digital application was further developed to provide health route planning for more than 7.5 million Hong Kong residents during their active mobility.

2. Materials and Methods

2.1. Data Sources

2.1.1. Ground-Level $PM_{2.5}$ Measurements

In the headed study, hourly $PM_{2.5}$ concentration data, from 1 January 2014 to 31 December 2021, were obtained from all 16 air quality monitoring stations (AQMS) in Hong Kong (Figure 1). These hourly $PM_{2.5}$ concentrations are based on high-accuracy gravimetric sampling, using the Thermal Scientific Model 1405-DF Filter Dynamics Measurement System (FDMS) from the Hong Kong Environment Protection Department (HKEPD) (Hohenberger et al., 2021; G. Shi et al., 2021).

2.1.2. Satellite Observations

A total of 56 Landsat 8 OLI/TIRS images during the Landsat 8 overpass time (10–11 a.m. in Hong Kong) from 1 January 2014 to 31 December 2021, was used in this above study. Landsat 8 has a spatial resolution of 30 m and a temporal resolution of 16-day. These 56 Landsat 8 images had almost no cloud cover and could be considered "fully clear images". In the traditional estimation of $PM_{2.5}$ by AOD, the AOD products are often retrieved from TOA reflectance of the blue band, the red band, and that at 2.13 μm via a dark-target-based algorithm (Shen

et al., 2018). Furthermore, the observation angles have been found to be important parameters regarding the physical relationship between TOA reflectance and surface $PM_{2.5}$ (Shen et al., 2018). Hence, the TOA on bands 2 (Blue: 0.45–0.51 μm), 4 (Red: 0.64–0.67 μm), and 7 (SWIR 2: 2.11–2.29 μm) and observation angles (i.e., sensor azimuth, sensor zenith, solar azimuth, and solar zenith) are obtained from the Landsat 8 data set to estimate $PM_{2.5}$. The technical details for converting DN values of Landsat 8 to TOA reflectance have been considered in the study of Mishra et al. (2021).

In addition, the normalized difference vegetation index (NDVI) during the same period was also estimated by band 4 and band 5 of Landsat 8 images (Ouzemou et al., 2018). The IBI during the same period was also estimated by band 3, band 4, band 5, and band 6 of Landsat 8 images (XI et al., 2019).

2.1.3. Meteorological Data

The $PM_{2.5}$ pollution in the urban environment is affected by meteorological factors. Thus, the Goddard Earth Observing System Forward Processing (GEOS-FP) meteorological data from 1 January 2014 to 31 December 2021, are incorporated in this study (Jiang et al., 2020; Yang et al., 2019). GEOS-FP has been successfully used in a previous study to estimate $PM_{2.5}$ from the satellite TOA reflectance (Shen et al., 2018). The meteorological data of GEOS-FP have a spatial resolution of 0.25° latitude × 0.3125° longitude. Local time (the Landsat 8 overpass time corresponds to 10:00–11:00 a.m.) was used. (a) Wind speed at 2 m above ground (WS, m/s), (b) air temperature at a 2-m height (TEMP, K), (c) surface pressure (PS, kPa), and (d) planetary boundary layer height (PBLH, m), were extracted from the GEOS-FP meteorological data between 10 and 11 a.m. local time.

2.1.4. Google Street View Images

The contribution of urban street-level greening in reducing PM2.5 concentrations has been proven by many studies (Cai et al., 2020; Wu et al., 2021; R. Zhang et al., 2021; Zhao et al., 2021). Neighborhoods that had higher green space coverage displayed lower PM2.5 concentrations. Hence, street-level greenness in Hong Kong was estimated through a novel GVI using GSV images. The methodology proposed by Li et al. was employed to calculate the GVI (Li et al., 2015). To calculate the GVI of each GSV point location, the following equation is used to calculate the proportion of green pixels in four images collected (Li et al., 2015):

$$GVI = \frac{\sum_{i=1}^{n=4} \frac{N_{g\_i}}{N_{t\_i}}}{4} \times 100\% \quad (1)$$

where N_{g_i} indicates the number of green pixels at the ith direction, and N_{t_i} indicates the total number of pixels at the ith direction. The GVI indicates the ratio of total green pixels from four pictures to the total pixels of the panoramic pictures. The GVI index is then used in the assessment of street-level greenery. To identify green pixels, the following equation is employed (Li et al., 2015):

$$Pi = \begin{cases} 0, \ if \ (Green_i - Blue_i) \times (Green_i - Red_i) < t \\ 1, \ if \ (Green_i - Blue_i) \times (Green_i - Red_i) > t \end{cases} \quad (2)$$

Where P_i indicates whether the ith pixel is a green pixel; Red_i, $Green_i$, and $Blue_i$ denote the red, green, blue channel values of the ith pixel; t is a threshold that determines whether the pixel is a green pixel. The threshold t is chosen by the OTSU algorithm automatically. The average value of the green pixel ratios in four street view images at a specific location is used regarding the measurement of the urban-street-level greenery.

2.1.5. Land Use Data

Hong Kong land use data has been used in this study. The land-use data includes 4 types of land use (Y. Shi et al., 2018): (a) Residential use (*lu_res*); (b) Commercial use (*lu_com*); (c) Government use (*lu_gov*); (d) Open space (*lu_ops*). In term of the total area (unit: m^2) regarding the land-use type of each of the 16 monitoring stations was calculated using the buffering analysis.

2.1.6. OpenStreetMap (OSM) and Bus Stop Points Data

To measure the impact of local road traffic density in Hong Kong in term of the local $PM_{2.5}$ pollution, five types of road lines density have been used in this study: (a) Primary, secondary, trunk road line density (*rd-main*); (b) Tertiary road line density (*rd-ter*); (c) Service road line density (*rd-ser*); (d) All motor vehicle roads line density

(*rd-all*); (e) All railway road line density (*rd-rai*). Based on the related OSM data (Z. Zhang et al., 2018), each of the five types of road line density was calculated separately. Additionally, and based on the official data of bus stop points, the closest distance to bus stops (CDS) was also calculated.

2.1.7. Urban Surface Factors Data

The outdoor $PM_{2.5}$ pollution is significantly affected by the urban form factors within the urban canopy layer, such as the mean height, the variation in building height, and the building density. Thus, to take into account the microscale urban form factor variations that affect the $PM_{2.5}$ estimation in a high-density city, a set of urban surface factors including SVF (G. Li et al., 2020), elevation, terrain slope, and terrain aspect were calculated using the buffer analysis. The buffer analysis was based on the Digital Terrain Models (DTM) data, building height data, and Google elevation data.

2.1.8. Commercial Restaurant and Temple Points Data

Cooking emissions from commercial restaurants are also outdoor sources for urban-community-level $PM_{2.5}$ (Lung et al., 2020; H. Xu et al., 2020). Of these emissions, barbecues and Chinese restaurants are the main sources of $PM_{2.5}$ pollution (Hsu et al., 2020). Thus, based on the points data of barbecues and Chinese restaurants, the impact of cooking emissions was calculated by using the buffering analysis, separately. In addition, more than 2 million people in Hong Kong, follow the Buddhist/Taoist religion, and during the periods of prayer incense and joss paper burnt in temples both during festival periods and as a common part of daily life (C. Chen et al., 2021; Hsu et al., 2020). Based on the points data of temples, the impact of incense/joss paper burning was calculated using buffering analysis.

2.2. TOA-LUR Modeling and Validation Methods

The TOA derived from the Landsat 8 images was used in combination with the traditional LUR modeling to estimate the microscale $PM_{2.5}$. The microscale meteorological factors and geographic predictors were incorporated in the TOA-LUR modeling. We resampled the meteorological data to match the satellite observations. All these data were reprojected to the same coordinate system. Finally, we extracted the satellite observations and related factors for the locations where $PM_{2.5}$ measurements were available.

First, the MLR method was adopted to identify the important predictor variables followed by the estimation of the microscale $PM_{2.5}$ (Tong et al., 2021). The geographically and temporally weighted regression (GTWR) model was also used. The TOA-LUR modeling process was conducted in the steps given below (Shi et al., 2018).

2.2.1. The Development of a Basic TOA-$PM_{2.5}$ Model

First, a basic model was developed to build the TOA-$PM_{2.5}$ correlation, with the latter mainly considering meteorological factors—Wind speed at 2 m above ground (WS), air temperature at a 2-m height (TEMP), surface pressure (PS), and planetary boundary layer height (PBLH) :

$$PM_{2.5ij} = b_1\mathrm{TOA}_{2\_ij} + b_2\mathrm{TOA}_{4\_ij} + b_3\mathrm{TOA}_{7\_ij} + b_4\mathrm{sat\_az}_{ij} + b_5\mathrm{sat\_zn}_{ij} + b_6\mathrm{sun\_az}_{ij} + b_7\mathrm{sun\_zn}_{ij} + b_8\mathrm{TEMP}_{ij} + b_9\mathrm{WS}_{ij} + b_{10}\mathrm{PS}_{ij} + b_{11}\mathrm{PBLH}_{ij} + \beta_{ij} + \varepsilon_{ij} \quad (3)$$

where $PM_{2.5ij}$ is the estimated $PM_{2.5}$ concentration at the $PM_{2.5}$ monitoring station i on day j. TOA_{2_ij}, TOA_{4_ij}, and TOA_{7_ij} are related TOA reflectances on bands 2, 4, and 7 (Blue, Red, and SWIR 2) of Landsat 8 at the location i on day j. sat_az_{ij}, sat_zn_{ij}, sun_az_{ij}, and sun_zn_{ij} are observation angles (i.e., sensor azimuth, sensor zenith, solar azimuth, and solar zenith) of Landsat 8 at the location i on day j. b_1, b_2, b_3, b_4, b_5, b_6, and b_7 are the slopes of TOA_{2_ij}, TOA_{4_ij}, TOA_{7_ij}, sat_az_{ij}, sat_zn_{ij}, sun_az_{ij}, and sun_zn_{ij}. b_8, b_9, b_{10}, and b_{11} are the slopes for the four daily basic weather variables. β_{ij} is the interception of the model. ε_{ij} is the residuals that presumably vary by day.

Unlike the behavior in the summer season, air pollution in Hong Kong during the winter season is affected not only by local emissions but also by the regional impact from the Guangdong-Hong Kong-Macao Greater Bay Area (Y. Shi et al., 2016). Thus, to distinguish seasonal changes, seasonal MLR correlation models are proposed to predict microscale $PM_{2.5}$ in each of the following periods: spring, summer, autumn, and winter.

2.2.2. Developing TOA-LUR MLR Models

In this study, a total of 210 potential explanatory variables have been used for buffer analysis. Included were 14 variables of 15 different buffer sizes. In the study, a series of regression analyses were conducted on each

buffer-based variable, to further enable sensitivity testing of the different buffer sized variables in the model. Some key variables for the TOA-LUR regression modeling were chosen to enable the prevention of over-fitting problems in the subsequent stepwise regression modeling process. The following regression analyses were conducted using the following model structure:

$$PM_{2.5ij} = b_1\mathrm{TOA}_{2\_\mathrm{ij}} + b_2\mathrm{TOA}_{4\_\mathrm{ij}} + b_3\mathrm{TOA}_{7\_\mathrm{ij}} + b_4\mathrm{sat\_az}_{ij} + b_5\mathrm{sat\_zn}_{ij} + b_6\mathrm{sun\_az}_{ij} + b_7\mathrm{sun\_zn}_{ij} + b_8\mathrm{TEMP}_{\mathrm{ij}} + b_9 WS_{\mathrm{ij}} + b_{10}\mathrm{PS}_{\mathrm{ij}} + b_{11}\mathrm{PBLH}_{\mathrm{ij}} + b_{12}\mathrm{VAR}_d + \beta_{ij} + \varepsilon_{ij} \quad (4)$$

Where b_1, b_2, b_3, b_4, b_5, b_6, and b_7 are the slopes of TOA_{2_ij}, TOA_{4_ij}, TOA_{7_ij}, sat_az_{ij}, sat_zn_{ij}, sun_az_{ij}, and sun_zn_{ij}. b_8, b_9, b_{10}, and b_{11} are the slopes for the four daily basic weather variables. b_{12} is the slope for the buffer-based variable (VAR_d) using the buffer size of d. For example, the tertiary road line density calculated in 750 m buffer and 1,500 m buffer are used as two separate variables. Specifically, d is set as 10, 20, 50, 100, 200, 300, 400, 500, 750, 1,000, 1,500, 2,000, 3,000, 4,000, and 5,000 m. The model performance was indicated by using Adjusted R^2. Furthermore, by using the "A Distance Decay Regression Selection Strategy (ADDRESS)" (Su et al., 2009), variables at the critical buffers were chosen as candidate explanatory variables. The identification details of critical buffers have been given in a previous study (Su et al., 2009). It has been also applied in two previous studies of Hong Kong (Shi et al., 2018; Tong et al., 2021).

The forward stepwise regression modeling was used to establish the TOA-LUR models during different seasons (Beelen et al., 2013). According to the minimum Bayesian Information Criterion (BIC), the model with the highest R^2 is selected. The variance inflation factor (VIF) regarding the total models is checked to eliminate collinearity problems in the resulting model. Variables with their p-value greater than 0.10 and VIF greater than 5 are excluded from the model (Vienneau et al., 2013). The final model can be expressed as

$$PM_{2.5\mathrm{ij}} = b_1\mathrm{TOA}_{2\_\mathrm{ij}} + b_2\mathrm{TOA}_{4\_\mathrm{ij}} + b_3\mathrm{TOA}_{7\_\mathrm{ij}} + b_4\mathrm{sat\_az}_{ij} + b_5\mathrm{sat\_zn}_{ij} + b_6\mathrm{sun\_az}_{ij} + b_7\mathrm{sun\_zn}_{ij} + \ldots + b_k\mathrm{VAR}_{k\mathrm{ij}} + \ldots + b_n\mathrm{VAR}_{d,n} + \beta_{ij} + \varepsilon_{ij} \quad (5)$$

where $PM_{2.5ij}$ is the predicted $PM_{2.5}$ concentration at the location of the air quality monitoring station i on day j. TOA_{2_ij}, TOA_{4_ij}, and TOA_{7_ij} are related TOA reflectances on bands 2, 4, and 7 of Landsat 8 at the location i on day j. sat_az_{ij}, sat_zn_{ij}, sun_az_{ij}, and sun_zn_{ij} are observation angles (i.e., sensor azimuth, sensor zenith, solar azimuth, and solar zenith) of Landsat 8 at the location i on day j. b_1, b_2, b_3, b_4, b_5, b_6, and b_7 are the slopes of TOA_{2_ij}, TOA_{4_ij}, TOA_{7_ij}, sat_az_{ij}, sat_zn_{ij}, sun_az_{ij}, and sun_zn_{ij}. $b_8 \ldots b_n$ are the slopes for the selected meteorological variables and the other candidate geographic variables. β_{ij} is the intercept of the TOA-LUR model. ε_{ij} is the residuals.

2.2.3. Developing TOA-LUR GTWR Models

The above TOA-LUR MLR model follows the structure of the fixed effects model. It is the influence of the predictor variables in these models which is temporally fixed. However, the influence of some predictor variables changes over time. Therefore, to further improve the TOA-LUR modeling, taking time-dependent random effects and geographic non-stationarity as important considerations, the TOA-LUR GTWR is applied to estimate microscale $\mathrm{PM}_{2.5}$ (Bai et al., 2016; Huang et al., 2010):

$$PM_{2.5\mathrm{ij}} = b_1\mathrm{TOA}_{2\_\mathrm{ij}} + b_2\mathrm{TOA}_{4\_\mathrm{ij}} + b_3\mathrm{TOA}_{7\_\mathrm{ij}} + b_4\mathrm{sat\_az}_{ij} + b_5\mathrm{sat\_zn}_{ij} + b_6\mathrm{sun\_az}_{ij} + b_7\mathrm{sun\_zn}_{ij} + \sum_k b_k(x_i, y_i, j)VAR_{kij} + \sum_k b_m(x_i, y_i, j)VAR_m + \beta_{ij} + \varepsilon_{ij} \quad (6)$$

where $PM_{2.5ij}$ is the estimated $\mathrm{PM}_{2.5}$ concentration at the $\mathrm{PM}_{2.5}$ monitoring station i on day j. TOA_{2_ij}, TOA_{4_ij}, and TOA_{7_ij} are the related TOA reflectance on bands 2, 4, and 7 of Landsat 8 at location i on day j. sat_az_{ij}, sat_zn_{ij}, sun_az_{ij}, and sun_zn_{ij} are observation angles (i.e., sensor azimuth, sensor zenith, solar azimuth, and solar zenith) of Landsat 8 at the location i on day j. b_1, b_2, b_3, b_4, b_5, b_6, and b_7 are the slopes of TOA_{2_ij}, TOA_{4_ij}, TOA_{7_ij}, sat_az_{ij}, sat_zn_{ij}, sun_az_{ij}, and sun_zn_{ij}. x_i, y_i are the geographical coordinates of the $\mathrm{PM}_{2.5}$ monitoring station i. b_k are the slopes for the k meteorological variables VAR_{kij}. b_m are the slopes for the m candidate geographic variables (VAR_m). β_{ij} and ε_{ij} are the intercept and residuals.

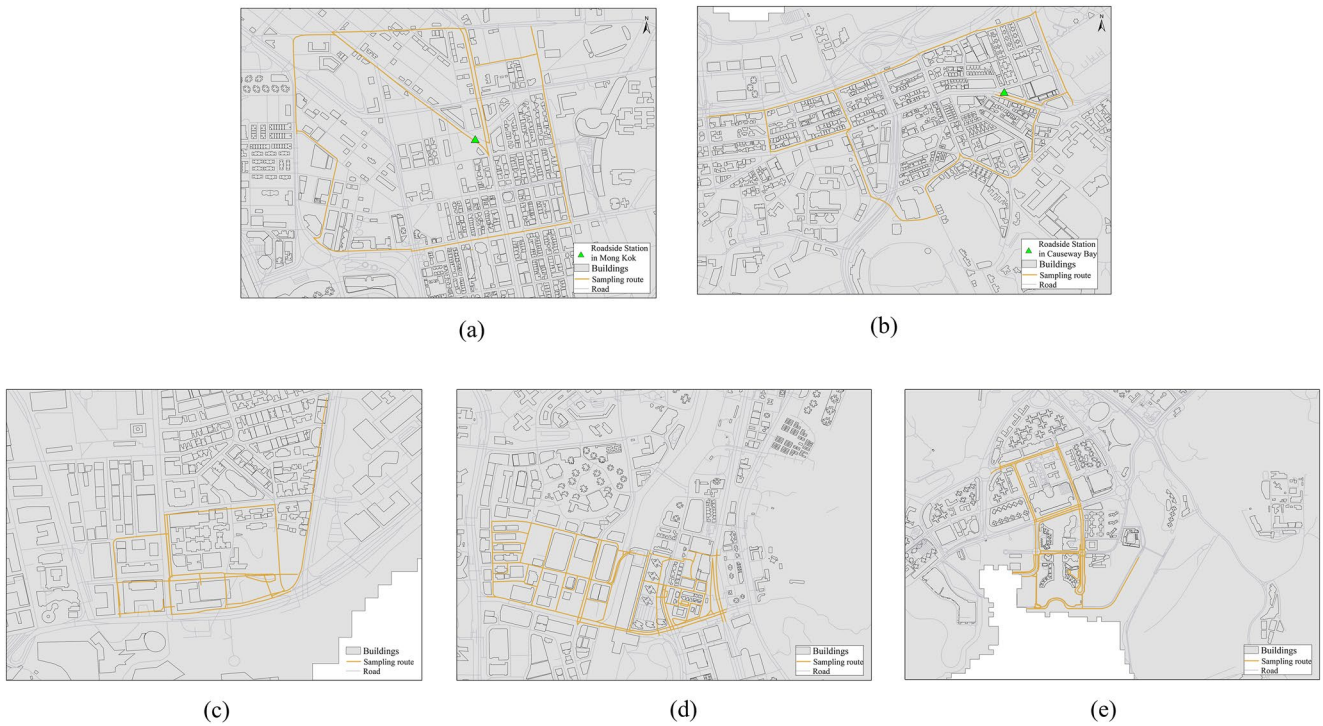

Figure 2. The sampling routes used by Airbeam2 for the external data validation. (a) The sampling routes around Mong Kok Station. (b) The sampling routes around Causeway Bay Station. (c) The sampling routes at Tsim Sha Tsui. (d) The sampling routes at Tuen Mun. (e) The sampling routes at Tseung Kwan O.

2.2.4. Model Validation

$\overline{R^2}$ and Root-mean-square error (RMSE) were chosen for testing both the model fit and the cross-validation. Among them, leave-one-out cross-validation (LOOCV) was used to validate these models. This validation process is repeated n times. The calculation method of $\overline{R^2}$ and RMSE is as follows:

$$\overline{R^2} = 1 - \left(1 - R^2\right)\left(\frac{n-1}{n-p-1}\right)$$
$$\mathrm{RMSE} = \sqrt{\frac{1}{n}\sum_{i=1}^{n}\left(PM_{2.5\_estimated_i} - PM_{2.5\_measured_i}\right)^2} \quad (7)$$

Where R^2 is the coefficient of determination of the models. n is the total number of measurement points. In the annual model, n is set as 699 in 56 days. In the seasonal models, n is set as (a) 164 during 14 days in spring, (b) 194 during 14 days in Summer, (c) 181 during 14 days in Autumn, and (d) 160 during 14 days in Winter. p is the total number of the selected prediction variables. $PM_{2.5\_measured_i}$ is the estimated $PM_{2.5}$ concentration. $PM_{2.5\_measured_i}$ is the measured $PM_{2.5}$ concentration.

2.2.5. External Model Validation

To better validate the models, the mobile measurement instruments - Airbeam2 were used to test the estimated results of the above TOA-LUR GTWR models on typical routes (a) near two roadside $PM_{2.5}$ measurement stations: one in Mong Kok and the other in Causeway Bay (Figures 2a and 2b), (b) at Tsim Sha Tsui, Tuen Mun, and Tseung Kwan O (Figures 2c–2e) far from the monitor stations. The background environment of these sampled roads covers high-density central urban areas (Mong Kok, Causeway Bay, and Tsim Sha Tsui) as well as the more open new towns (Tuen Mun, Tseung Kwan O). The testing experiments were carried out simultaneously during the Landsat-8 transit time in Hong Kong during the period: 2019 and 2021. The prediction performance of the TOA-LUR GTWR model was evaluated by comparing four seasonal $PM_{2.5}$ estimation results with the actual $PM_{2.5}$ results measured by Airbeam2. In order to reduce the accidental error of Airbeam2 in the mobile measurement, the average concentration of the measurement of two Airbeam2 was used as the actual $PM_{2.5}$ concentration. In addition, the precision test of Airbeam2 in Hong Kong was conducted by comparing the mobile measurement

Table 1
Precision Test of Airbeam2 Compared With the Two Roadside $PM_{2.5}$ Monitoring Stations of Environmental Protection Department

Time periods	$PM_{2.5}$(μg/m^3) *X*-axis	$PM_{2.5}$(μg/m^3) *Y*-axis	Linear regression	R^2
Spring	Airbeam2	Causeway Bay station	$Y = 0.9144X + 1.7944$	0.91
	Airbeam2	Mong Kok station	$Y = 0.9261X + 1.4207$	0.92
Summer	Airbeam2	Causeway Bay station	$Y = 0.9136X + 1.8292$	0.97
	Airbeam2	Mong Kok station	$Y = 0.9868X + 1.2512$	0.98
Autumn	Airbeam2	Causeway Bay station	$Y = 0.9584X + 1.2205$	0.92
	Airbeam2	Mong Kok station	$Y = 0.9452X + 0.9935$	0.92
Winter	Airbeam2	Causeway Bay station	$Y = 0.8498X + 1.4676$	0.90
	Airbeam2	Mong Kok station	$Y = 0.9419X + 1.3123$	0.90

values of Airbeam2 with the completed static measurement values of Mong Kok and Causeway Bay stations at the same locations. The results of the precision test are shown in Table 1.

2.3. Healthy Route Searching

An undirected graph $R = (X, Z, W_{PM2.5})$, including X nodes, Z related edges, and the weights of edges -$W_{PM2.5}$. The weight W_p represented the $PM_{2.5}$ pollution weight of the edges. The example of the $PM_{2.5}$ weight calculation method is shown in Figure 3. X_1 and X_2 were connected by an edge Z_1 located in three grids. In three grids, the estimated $PM_{2.5}$ concentrations by TOA-LUR modeling are v_1, v_2, and v_3 respectively. The calculation formula for the weight $W_{PM2.5}$ is (Tong et al., 2021):

$$W_{PM2.5} = d_{1,1} \times v1 + d_{1,2} \times v2 + d_{1,3} \times v3 \quad (8)$$

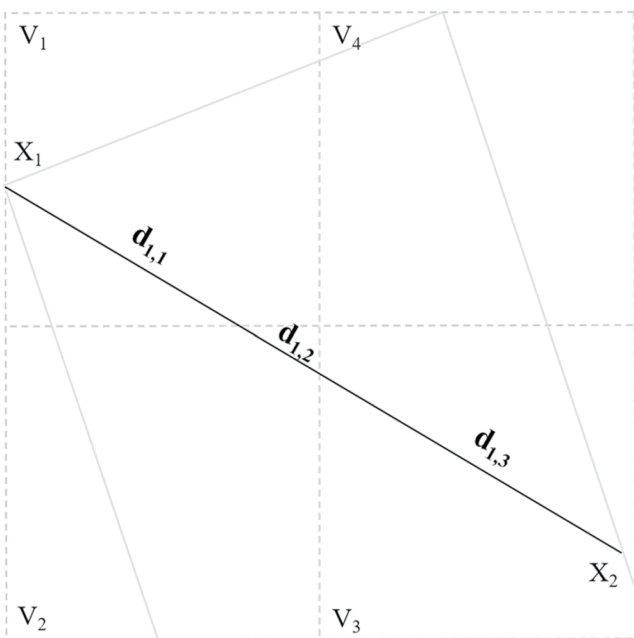

Figure 3. The example of $PM_{2.5}$ weight calculation method. X_1 and X_2 were connected by an edge Z_1 located in three grids. In three grids, the estimated $PM_{2.5}$ concentrations by TOA-LUR modeling are v_1, v_2, and v_3 respectively. $d_{1,1}$ is the length of edge Z_1 in grid 1. $d_{1,2}$ is the length of edge Z_1 in grid 2. $d_{1,3}$ is the length of edge Z_1 in grid 3.

where $d_{1,1}$ is the length of edge Z_1 in grid 1, $d_{1,2}$ is the length of edge Z_1 in grid 2, and $d_{1,3}$ is the length of edge Z_1 in grid 3.

Based on the example of the $PM_{2.5}$ weight calculation method, the $PM_{2.5}$ weight of all edges of the road network throughout the whole city could be obtained. The typical A* pathfinding algorithm (Szczerba et al., 2000) is then, used to extract the healthy travel route with the lowest $PM_{2.5}$ cost. A* pathfinding algorithm is an acceptable heuristic search algorithm, which never overestimates the cost of reaching the destination node. Further, it can be used to quickly find the route with the lowest cost.

3. Results

3.1. TOA-$PM_{2.5}$ Models

Based on the Landsat 8 data, ground monitoring point data, and meteorological data from 2014 to 2019, MLR models of basic TOA-$PM_{2.5}$ in the annual year, spring, summer, autumn, and winter were developed. In order to illustrate the performance of these MLR models, the TOA-only model (only TOA and related observation angles are considered to estimate $PM_{2.5}$) was developed as a reference. The performance results of these models are shown in Table 2. The results show that, compared to the TOA-only model, the basic TOA-$PM_{2.5}$ MLR models perform better in the prediction of the ground-level $PM_{2.5}$ in Hong Kong (Table 2). However, the performance of these TOA-$PM_{2.5}$ MLR models is still poor as regards the prediction of the ground-level $PM_{2.5}$ during each season throughout the annual year. The

Table 2
The List of Resultant Baseline Models by Seasons and Improved TOA-LUR MLR Models

		Models	Estimated performance					
			R^2	$\overline{R^2}$	Fitting-RMSE (μg/m^3)	$LOOCV - \overline{R^2}$	LOOCV-RMSE (μg/m^3)	p
TOA-only model	Annual	11.05*TOA2-3.90*TOA4-3.43*TOA7-0.01*sat_az- 2.29*sat_zn+0.11*sun_az+0.26*sun_zn+231.55	0.20	0.19	18.11	0.19	18.38	<0.0001*
TOA-$PM_{2.5}$ MLR models	Annual	16.18*TOA4-7.58*TOA2-3.88*TOA7-0.02*sat_az-2.24*sat_zn+0.21*sun_az+0.49*sun_zn-0.65*TEMP+0.15*WS-0.03*PBLH-0.01*PS-1348	0.24	0.22	18.04	0.20	18.39	<0.0001*
	Spring	56.59*TOA4-71.54*TOA2+5.51*TOA7-0.05*sat_az-3.60*sat_zn-1.57*sun_az+0.31*sun_zn-2.09*TEMP+5.51*WS-0.02*PBLH-0.01*PS+384.6	0.38	0.32	16.01	0.31	16.34	<0.0001*
	Summer	11.54*TOA2-7.37*TOA4-5.20*TOA7-0.01*sat_az+0.002*sat_zn-0.03*sun_az-0.17*sun_zn+1.83*TEMP+1.32*WS-0.01*PBLH+0.003*PS-681	0.40	0.37	16.32	0.36	16.92	<0.0001*
	Autumn	12.23*TOA2+4.09*TOA4-15.87*TOA7-0.12*sat_az-3.89*sat_zn+6.52*sun_az-6.68*sun_zn+6.94*TEMP+14.28*WS-0.05*PBLH-0.01*PS-1298	0.35	0.34	15.41	0.33	16.13	<0.0001*
	Winter	18.98*TOA2-14.24*TOA4+3.53*TOA7-0.002*sat_az-0.50*sat_zn-0.28*sun_az-0.15*sun_zn-0.71*TEMP-0.40*WS-0.001*PBLH-0.01*PS+561	0.26	0.24	16.21	0.22	16.46	<0.0001*
TOA-LUR MLR models	Annual	−109.6*NDVI-0.02*PBLH-0.03*PS+16.34*TOA2-7.11*TOA4-1.51*TOA7-0.02*sat_az-0.48*sat_zn+0.30*sun_az+0.41*sun_zn-0.49*TEMP-0.69*WS-98.6*SVF-2.13*slope-37.14*GVI+0.01*CDS+0.13*rd-main-0.002*lu-ops+4673	0.43	0.36	16.83	0.35	17.13	<0.0001*
	Spring	−45.12*NDVI-0.02*PBLH-0.01*PS+30.12*TOA2-20.54*TOA4-9.87*TOA7-0.08*sat_az-0.49*sat_zn-0.43*sun_az+3.90*sun_zn+2.01*TEMP+3.23*WS+0.50*Elevation+642.1*SVF+0.32*slope-10.86*GVI+0.01*temple+25.13*BR+0.01*CDS+0.04*rd-main-0.02*rd-rai-0.002*lu-gov-0.001*lu-com-0.002*lu-ops-1714	0.56	0.45	15.43	0.43	15.54	<0.0001*
	Summer	−11.88*NDVI-0.01*PBLH+0.01*PS+13.14*TOA2-8.34*TOA4-6.01*TOA7 +0.04*sat_az+0.06*sat_zn+0.21*sun_az-1.32*sun_zn+2.75*TEMP+2.32*WS+0.52*Elevation+1104*SVF+1.73*slope-14*GVI+0.01*BR+0.004*CR–0.01*CDS-0.03*rd-main+0.07*rd-rai +0.05*rd-ter-0.001*lu-ops-8478	0.64	0.55	13.34	0.54	13.51	<0.0001*
	Autumn	0.02*PS+19.38*TOA2-13.09*TOA4-3.84*TOA7-0.14*sat_az-1.59*sat_zn+ 7.98*sun_az-6.57*sun_zn+16.28*TEMP+19.34*WS-897.4*SVF-2.15*GVI-0.002*CDS-0.001*lu_open-0.01*lu_res-0.002*lu_com-2138	0.59	0.53	13.81	0.51	14.03	<0.0001*
	Winter	−23.21*NDVI-0.002*PS+11.32*TOA2+0.81*TOA4-3.02*TOA7-0.004*sat_az-0.29*sat_zn+0.03*sun_az-0.18*sun_zn-0.62*TEMP-0.58*WS-458.6*SVF-0.59*slope-38.62*GVI-0.001*CDS+0.01*CR+0.01*temple-0.03*rd_main-0.01*rd_rai-0.02*rd_ter-3715	0.50	0.44	15.68	0.41	15.82	<0.0001*

LOOCV $\overline{R^2}$ value of the annual TOA-$PM_{2.5}$ MLR model is lower than 0.2 (Table 2). The LOOCV $\overline{R^2}$ values of the spring, summer, autumn, and winter TOA-$PM_{2.5}$ MLR models are 0.21–0.36 (Table 2).

3.2. TOA-LUR MLR Models

Based on the above-mentioned basic TOA-$PM_{2.5}$ MLR models, by combining the microscale geographic prediction factors, the TOA-LUR MLR models were developed to improve the performance for ground-level $PM_{2.5}$ prediction. The testing results (Table 2) show that the prediction performances of TOA-LUR MLR models are

Table 3
The Performance of TOA-LUR MLR Models With and Without the GVI Index

		Performance (with the GVI index)						Performance (without the GVI index)					
		R^2	$\overline{R^2}$	Fitting-RMSE (μg/m^3)	$LOOCV - \overline{R^2}$	LOOCV-RMSE (μg/m^3)	p	R^2	$\overline{R^2}$	Fitting-RMSE (μg/m^3)	$LOOCV - \overline{R^2}$	LOOCV-RMSE (μg/m^3)	p
TOA-LUR MLR models	Annual	0.43	0.36	16.83	0.36	17.13	<0.0001*	0.40	0.34	17.27	0.31	17.41	<0.0001*
	Spring	0.56	0.45	15.43	0.43	15.54	<0.0001*	0.52	0.41	16.39	0.41	16.48	<0.0001*
	Summer	0.64	0.55	13.34	0.53	13.51	<0.0001*	0.60	0.48	14.46	0.45	14.83	<0.0001*
	Autumn	0.59	0.53	13.81	0.51	14.03	<0.0001*	0.56	0.45	15.02	0.44	15.60	<0.0001*
	Winter	0.50	0.44	15.68	0.41	15.82	<0.0001*	0.49	0.40	16.43	0.39	16.60	<0.0001*

higher than those of the basic TOA-$PM_{2.5}$ MLR models. Among these models, the LOOCV R^2 for the annual TOA-LUR MLR models increased to 0.35 (Table 2). The prediction performances for the TOA-LUR MLR model in spring, summer, autumn, and winter were better. Th LOOCV $\overline{R^2}$ of these models were increased to 0.41–0.54 (Table 2). The details of the selected variables of the TOA-LUR MLR model are shown in Table S1. It is worth noting that only a few studies have introduced the GVI index as a predictor into the LUR model, to predict street-scale $PM_{2.5}$. Among the above models in this study, the GVI factor has acted as an important predictor in each of the annual and the four seasonal TOA-LUR MLR models. When incorporating the GVI index, the LOOCV $\overline{R^2}$ of annual and seasonal models could be increased by 7.16%–19.29% (Table 3).

3.3. TOA-LUR GTWR Models

The addition of consideration of time effects and geographic non-stationarity features into the model, enables the annual and four seasonal TOA-LUR GTWR models to be further developed and thereby improve the accuracy of $PM_{2.5}$ prediction (Table 4). The prediction accuracy in both annual and four seasonal TOA-LUR GTWR models has been improved significantly (LOOCV-R^2 was increased by 62.18%–70.14%). Among these models, the LOOCV R^2 for the summer TOA-LUR GTWR model reached 0.90 (Table 4). In particular, the GVI also played an important role in annual and four seasonal TOA-LUR GTWR models by increasing the LOOCV R^2 by 2.09%–4.22% (Table 4). Even when compared to other studies using the improved LUR model to estimate $PM_{2.5}$, the TOA-LUR GTWR models established in this study have achieved a better $\overline{R^2}$ (Table 5).

Of additional interest, is that verification of this study has, in turn, also verified the prediction results (Table 6) of the TOA-LUR GTWR model over four seasons concerning (a) the routes near the two roadside AQMS, one in Mong Kok and one in Causeway Bay (ultra-high-density central area of Hong Kong), (b) the routes without roadside monitoring stations nearby, that is, in Tsim Sha Tsui (business and leisure center area), Tuen Mun (new town), and Tseung Kwan O (new town). The above test routes cover the main high active mobility hotspots in Hong Kong. The mobile measurement instruments - Airbeam2 were used to test the prediction performance of

Table 4
The Performance of TOA-LUR GTWR Models With and Without the GVI Index

		Performance (with the GVI index)						Performance (without the GVI index)					
		R^2	$\overline{R^2}$	Fitting-RMSE (μg/m^3)	$LOOCV - \overline{R^2}$	LOOCV-RMSE (μg/m^3)	p	R^2	$\overline{R^2}$	Fitting-RMSE (μg/m^3)	$LOOCV - \overline{R^2}$	LOOCV-RMSE (μg/m^3)	p
TOA-LUR GTWR models	Annual	0.62	0.60	12.56	0.59	12.79	<0.0001*	0.61	0.59	13.64	0.58	13.94	<0.0001*
	Spring	0.75	0.72	11.39	0.72	11.58	<0.0001*	0.71	0.70	12.67	0.69	12.92	<0.0001*
	Summer	0.92	0.90	9.26	0.90	9.43	<0.0001*	0.89	0.88	9.71	0.86	9.90	<0.0001*
	Autumn	0.86	0.84	10.40	0.83	10.46	<0.0001*	0.83	0.81	10.85	0.81	11.13	<0.0001*
	Winter	0.74	0.72	12.02	0.70	12.16	<0.0001*	0.71	0.68	13.20	0.68	13.42	<0.0001*

Table 5
Performance Comparison of Improved TOA-LUR GTWR Models With Other Applications of Land Use Regression Models

Study	Study area	Season	$\overline{R^2}$
Mo et al. (2021)	Guangzhou	Spring	0.60
		Summer	0.56
		Autumn	0.62
		Winter	0.80
Shi et al. (2018)	Hong Kong	Spring	0.62
		Summer	0.90
		Autumn	0.71
		Winter	0.64
Chen et al. (2021)	Taiwan	Spring	0.68
		Summer	0.71
		Autumn	0.67
		Winter	0.80
Li et al. (2018)	Beijing	Spring	0.74
		Summer	0.50
		Autumn	0.68
		Winter	0.79
Lee et al. (2016)	California	Spring	0.57
		Summer	0.43
		Autumn	0.63
		Winter	0.69
This study	Hong Kong	Spring	0.72
		Summer	0.90
		Autumn	0.84
		Winter	0.72

the above TOA-LUR GTWR models on these above routes (Figures 2a–2e). From the testing results of the four seasons on the sampling roads in the above five areas, the R^2 for the four seasonal calibrations still remained at 0.67–0.89 (Table 6). This shows that seasonal TOA-LUR GTWR models perform well in the $PM_{2.5}$ estimation in different background environments.

3.4. Obtaining On-Road $PM_{2.5}$ Maps at High Spatial Resolution

The relevant seasonally on-road $PM_{2.5}$ spatial distribution maps were averaged, based on the daily $PM_{2.5}$ estimations derived from above TOA-LUR GTWR models (Figure 4). The on-road $PM_{2.5}$ distribution maps cover 70,788 roads in Hong Kong. It can be seen from the $PM_{2.5}$ distribution maps that the roads in Central, Causeway Bay, Mong Kok, and Sham Shui Po, all of which are in the central urban area, are more polluted by $PM_{2.5}$. The above-mentioned areas are also key areas for air pollution prevention and control in Hong Kong (Li & Feng, 2018). In addition, this study also shows that Tuen Mun had severe $PM_{2.5}$ pollution. The traffic volume on the roads in Tuen Mun area was usually high. However, this area is vulnerable to the air pollution of the Pearl River Delta, due to its geographical location. Thus, from the maps, it can be seen that the on-road $PM_{2.5}$ concentration in this area was particularly high in the winter. In summer, when local air pollution was dominated, on-road $PM_{2.5}$ concentration there was relatively low. The above results show that the TOA-LUR GTWR models proposed by this study can not only identify the hot spots of $PM_{2.5}$ pollution, but also show the seasonal differences in $PM_{2.5}$ pollution. Therefore, the TOA-LUR GTWR models proposed in this study can provide a reliable estimation of on-road $PM_{2.5}$ in the complex environment of high-density cities.

3.5. Developing the Healthy Route Planning App

Based on the mapping results of on-road $PM_{2.5}$ in Hong Kong and the health route searching method, a healthy route planning app was further developed, to provide the healthy travel route (including walking, running, and cycling) with less $PM_{2.5}$ in Hong Kong. A typical example is shown in Figure 5. The example indicates the healthy travel route and the shortest route from the HONG KONG Polytechnic University to the Hong Kong Metropolitan University. The healthy travel route is 100m more than the shortest route but the $PM_{2.5}$ pollution on the healthy travel route showed a decrease of 5.12%–10.58% over the four seasons. Furthermore, according to the $PM_{2.5}$ exposure reduction of 15 typical route planning examples in Hong Kong, healthy route planning could reduce the $PM_{2.5}$ exposure by 4.79%–25.08%, compared with the shortest route planning (Table 7). As a result, people, during their daily travel, can reduce their exposure to $PM_{2.5}$ pollution.

4. Conclusions

No matter where we live or how we travel, everyone begins and ends each trip as a pedestrian. In cities across the world, many people rely almost exclusively on walking and cycling to get to their destinations. The UN Environment Programme is calling for the development of new solutions that ensure that people who walk and cycle are able to experience improved physical health, and reduced air pollution (United Nations Environment Programme, 2020). Therefore, proposed is a framework that combines satellite observations and microscale geographic predictors to predict on-road $PM_{2.5}$ to assist healthy travel planning with less pollution to promote active mobility.

The results of the application of the proposed framework in Hong Kong reflect its characteristics in the following aspects:

1. The assurance of people's needs regarding healthy travel. The current existing route planning applications are mainly based on periods of time or road conditions for planning, and lastly lack of environmentally friendly

Table 6
Prediction Test From Seasonal TOA-LUR GTWR Models and Measurements by Airbeam2 on the Sampling Routes of Hong Kong

Time periods	$PM_{2.5}(\mu g/m^3)$ *X*-axis	$PM_{2.5}(\mu g/m^3)$ *Y*-axis	Linear regression	R^2
Spring	Estimations in Mong Kok	Airbeam2 in Mong Kok	$Y = 0.8463X + 1.8336$	0.71
	Estimations in Causeway Bay	Airbeam2 in Causeway Bay	$Y = 0.8264X + 2.9915$	0.69
	Estimations in Tsim Sha Tsui	Airbeam2 in Tsim Sha Tsui	$Y = 0.8246X + 2.3258$	0.69
	Estimations in Tuen Mun	Airbeam2 in Tuen Mun	$Y = 0.8422X + 1.8336$	0.70
	Estimations in Tseung Kwan O	Airbeam2 in Tseung Kwan O	$Y = 0.5715X + 5.6394$	0.68
Summer	Estimations in Mong Kok	Airbeam2 in Mong Kok	$Y = 0.991X + 0.0165$	0.89
	Estimations in Causeway Bay	Airbeam2 in Causeway Bay	$Y = 0.9244X + 1.1708$	0.88
	Estimations in Tsim Sha Tsui	Airbeam2 in Tsim Sha Tsui	$Y = 0.921X + 0.9719$	0.87
	Estimations in Tuen Mun	Airbeam2 in Tuen Mun	$Y = 0.9255X + 1.1793$	0.88
	Estimations in Tseung Kwan O	Airbeam2 in Tseung Kwan O	$Y = 0.9621X + 0.32$	0.88
Autumn	Estimations in Mong Kok	Airbeam2 in Mong Kok	$Y = 0.8102X + 2.9568$	0.83
	Estimations in Causeway Bay	Airbeam2 in Causeway Bay	$Y = 0.8556X + 2.2829$	0.82
	Estimations in Tsim Sha Tsui	Airbeam2 in Tsim Sha Tsui	$Y = 0.8397X + 3.3487$	0.81
	Estimations in Tuen Mun	Airbeam2 in Tuen Mun	$Y = 0.9046X + 0.6963$	0.83
	Estimations in Tseung Kwan O	Airbeam2 in Tseung Kwan O	$Y = 0.8642X + 1.6912$	0.80
Winter	Estimations in Mong Kok	Airbeam2 in Mong Kok	$Y = 0.7167X + 10.256$	0.70
	Estimations in Causeway Bay	Airbeam2 in Causeway Bay	$Y = 0.6617X + 12.904$	0.68
	Estimations in Tsim Sha Tsui	Airbeam2 in Tsim Sha Tsui	$Y = 0.6928X + 6.6171$	0.68
	Estimations in Tuen Mun	Airbeam2 in Tuen Mun	$Y = 0.834X + 1.8524$	0.69
	Estimations in Tseung Kwan O	Airbeam2 in Tseung Kwan O	$Y = 0.7324X + 5.0851$	0.67

route planning. Based on the microscale $PM_{2.5}$ estimation and high-resolution mapping of more than 70,000 roads in Hong Kong, a digital application providing healthy route planning has been developed. As a result, ensured has been the traveling health during the active mobility of all residents in Hong Kong. Furthermore, a feasible reference for healthy travel route planning has been provided for other regions.

2. Improved the correlation of TOA-$PM_{2.5}$ for the LUR models of spatiotemporal $PM_{2.5}$ estimation in the high-density city. The previous $PM_{2.5}$ estimation research related to the LUR model (including the model combining LUR and AOD) can cover a large spatial range (such as national or regional scale), but cannot support a sufficiently high spatial resolution (especially below 100 m) to reflect the spatial variation of micro $PM_{2.5}$ pollution within the city. In this study, by using TOA-LUR modeling to consider micro-scale geographic predictors including new factors such as GVI, the spatiotemporal correlation between TOA and ground $PM_{2.5}$ was effectively enhanced. This makes the spatial estimation of $PM_{2.5}$ more accurate, thus further supporting the acquisition of high spatial resolution micro-scale $PM_{2.5}$ distribution maps in the entire city.
3. Provides a fine-scale mapping of the spatiotemporal distribution of on-road $PM_{2.5}$ based on TOA-LUR modeling. These maps provide useful information for healthy route navigation and air pollution prevention by identifying more greatly refined $PM_{2.5}$ hotspots. The latter is critical for high-density cities with further complex environments such as Hong Kong. This also complements the shortcomings of the only three roadside inspection stations in the central area of Hong Kong. Thus, TOA-LUR modeling and geographic mapping technologies remote sensing data can be used to fill in the gaps of existing monitoring networks and help public health applications on a finer spatial scale. This study is the first application case in which TOA-LUR modeling is used to estimate on-road $PM_{2.5}$ in an ultra-high-density city, even though the established TOA-LUR model cannot be directly transferred to other places. However, it is clear and of value that the framework proposed in this study provides a generalizable method for the refined estimation of air pollution in high-density cities. Thus, relevant policy makers can make direct reference directly to it and use local data to adjust and further develop the model, to better enable a more comprehensive understanding of the differences

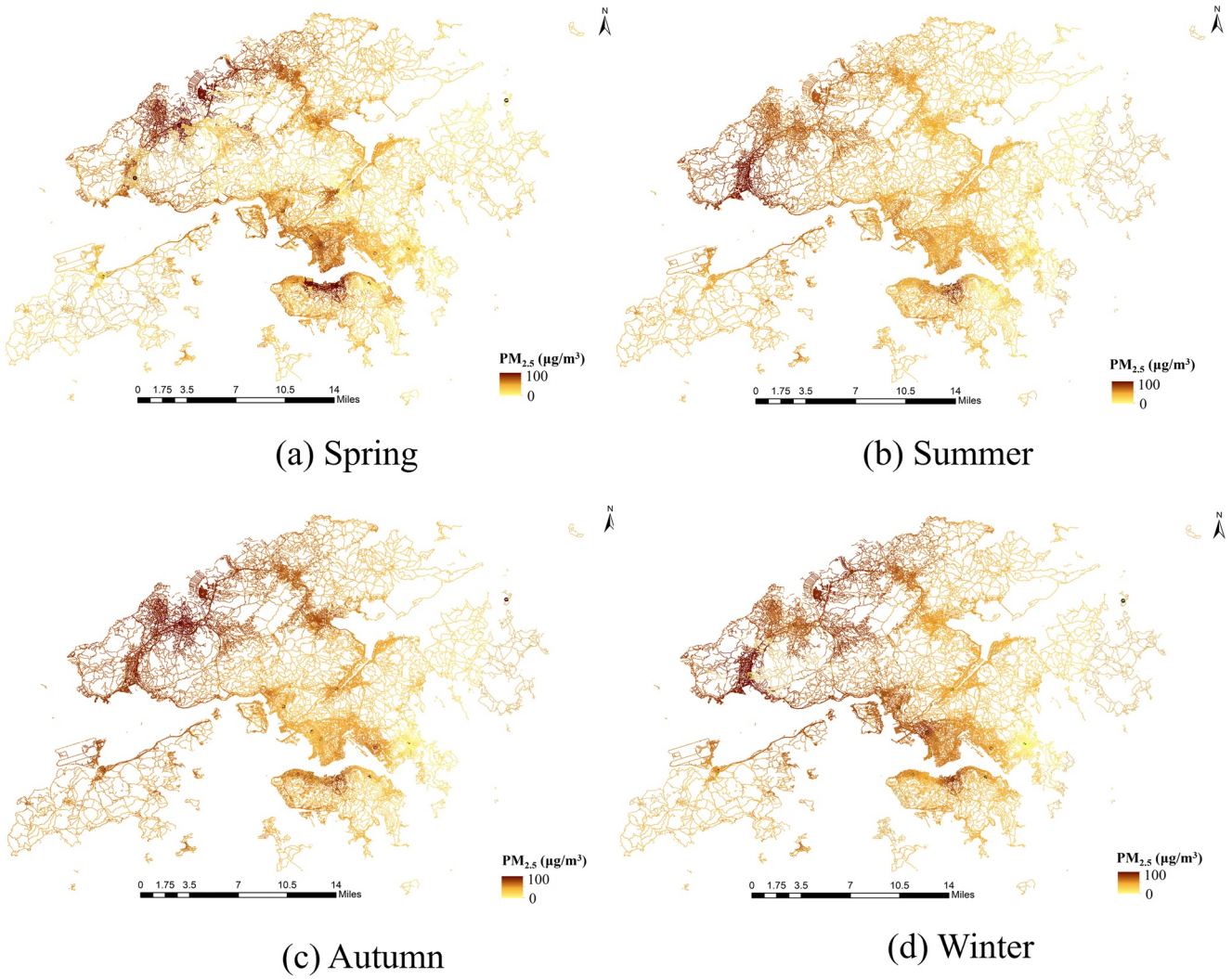

Figure 4. $PM_{2.5}$ distribution maps on 70, 788 roads of Hong Kong obtained by seasonal TOA-LUR GTWR models. (a) $PM_{2.5}$ distribution in Spring. (b) $PM_{2.5}$ distribution in Summer. (c) $PM_{2.5}$ distribution in Autumn. (d) $PM_{2.5}$ distribution in Winter.

in $PM_{2.5}$ in different areas of the high-density city. In addition, the applicability of the framework in other cities with less traffic needs to be further explored.

In order to assist people to travel more healthily during the active mobility, proposed is a framework to assist in the planning of healthy routes exposed to less $PM_{2.5}$, by estimating $PM_{2.5}$ at the high-spatial-resolution. First, based on the long-term observational data from 2014 to 2021 and the data on micro-geographical predictors, TOA-LUR models were developed to predict the spatiotemporal $PM_{2.5}$ distribution. Based on TOA-LUR models, the daily fine-scale spatiotemporal distribution of on-road $PM_{2.5}$ in Hong Kong was mapped. Further, by a healthy route search algorithm, an application that provides healthy travel route planning was developed. As a result, the framework has been used to assist Hong Kong's more than 7.5 million residents in healthy active mobility.

This study does have some limitations. Firstly, due to limitations in the availability of the data, especially the Landsat 8 data, this study can currently only estimate on-road $PM_{2.5}$ in the time frame of satellite transit from 10 to 11 a.m. each morning. The route planning services provided by the related healthy travel route planning applications are mainly for the morning rush hour travel in Hong Kong. After that, this study will further combine the satellite and ground-based multi-source pollution monitoring data with the higher spatiotemporal resolution to perform spatiotemporal fusion to estimate more refined $PM_{2.5}$, to serve for the healthy route

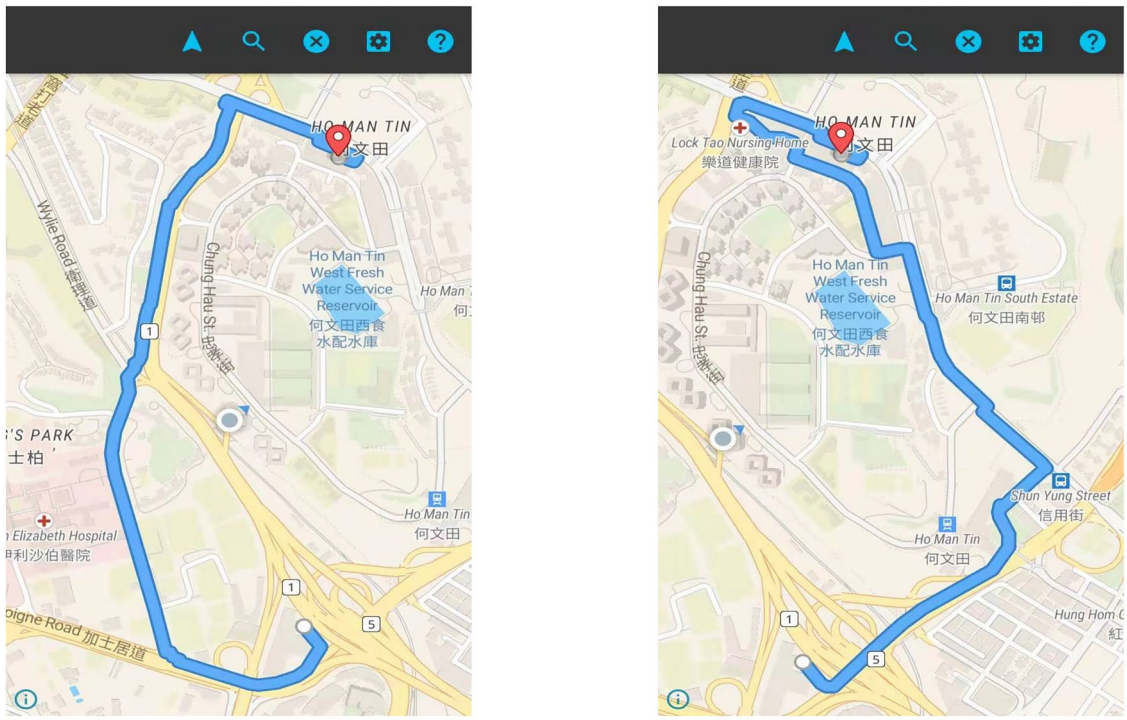

(a) Healthy travel route (b) Shortest travel route

Figure 5. The example of the healthy travel route planning from the HONG KONG Polytechnic University to the Hong Kong Metropolitan University.

traveling during more time periods. Secondly, the direct estimation of $PM_{2.5}$ from TOA reflectance is a very complicated process, especially for the nonlinear physical process. This study will consider applying the deep learning model to $PM_{2.5}$ estimation based on TOA reflectance at the urban fine-scale scale to further improve the estimation accuracy.

Table 7
The $PM_{2.5}$ Exposure Reduction of the Healthy Travel Route Compared With the Shortest Travel Route

Area	Route	$PM_{2.5}$ reduction (%)			
		Spring	Summer	Autumn	Winter
Wan Chai	Kew Green Hotel Wanchai - Wan Chai Sports Ground	11.52	13.02	11.79	8.68
	Hong Kong Arts Centre–Tung Shing Building	12.19	14.01	11.95	9.46
	United Centre - Wan Chai Market	13.07	13.95	13.45	10.23
	Cheong Ip Building - JEMS Character Academy	10.43	11.06	10.67	6.51
	Bakehouse - Harbour Centre	15.36	16.59	15.78	12.17
Tsim Sha Tsui	Kowloon Park - The Royal Garden	13.15	14.87	13.47	9.95
	iSQUARE - The Luxe Manor	9.78	10.34	9.43	5.17
	Hyatt Regency Hong Kong - East Ocean Centre	11.23	11.78	11.36	8.52
	InterContinental Grand Stanford Hong Kong - Hong Kong Observatory	8.22	10.05	8.54	4.79
	Tsim Sha Tsui Baptist Church - Harbour City	10.96	11.52	11.23	6.98
Tuen Mun	On Ting Estate - Tin Hau Temple Plaza	19.01	21.65	19.42	17.02
	Chelsea Heights Plaza - Tsing Tin Playground	24.17	25.08	24.63	22.96
	Tai Hing Estate Hing Yiu House - New Life Farm	22.47	24.01	23.75	19.12
	Tuen Mun San Hui Market - Hotel COZi Resort	18.69	19.42	18.96	17.25
	Tin's Centre - Waldorf Garden Tuen Mun	21.35	21.89	21.17	18.04

Every year, exposure to outdoor air pollution is estimated by World Health Organization (World Health Organization, 2021) to cause 7 million premature deaths and result in the loss of millions more healthy years of life. This mortality is due to exposure to $PM_{2.5}$ in outdoor activities. As a result, the WHO calls on countries around the world to establish planning tools to support people's healthier and cleaner daily travel. Although there are some limitations, the original framework proposed in this study provides an estimation and a mapping of on-road $PM_{2.5}$ at the fine scale, providing people with healthier travel choices. It may become a reference and guide for high-density cities, for smart travel planning, and refined monitoring of air pollution in urban areas. It is hoped, therefore, that this study assists more people in urban areas to reduce their exposure to outdoor air pollution, both to protect their health, and assist in the construction of healthy cities, especially for the high-density city.

Conflict of Interest

The authors declare no conflicts of interest relevant to this study.

Data Availability Statement

Data on $PM_{2.5}$ Monitoring Data can be accessed at https://cd.epic.epd.gov.hk/EPICDI/air/download/ by choosing the data set of fine suspended particulates in 16 stations of Hong Kong. Landsat 8 data can be accessed at https://earthexplorer.usgs.gov/ by choosing the geocoder as Hong Kong and the Landsat 8 OLI/TIRS C1 Level 1 in data sets. Meteorological data can be accessed at https://portal.nccs.nasa.gov/datashare/gmao/geos-fp/das/. Google Street View images can be accesses at https://www.google.com/streetview/. OpenStreetMap data can be accessed at https://www.openstreetmap.org/#map=10/22.3567/114.1363. The Digital Terrain Models (DTM) data can be accessed at https://data.gov.hk/en-data/dataset/hk-landsd-openmap-5m-grid-dtm. Building height data can be accessed at https://www.landsd.gov.hk/en/survey-mapping/mapping/3d-mapping.html. Google elevation data can be accessed at https://developers.google.com/maps/documentation/javascript/elevation.

Acknowledgments
This study was supported by National Key R&D Program of China (2019YFB2103102), and Otto Poon Charitable Foundation Smart Cities Research Institute, The Hong Kong Polytechnic University (Work Program: CD03).

References

Bai, Y., Wu, L., Qin, K., Zhang, Y., Shen, Y., & Zhou, Y. (2016). A geographically and temporally weighted regression model for ground-level $PM_{2.5}$ estimation from satellite-derived 500 m resolution AOD. *Remote Sensing*, *8*(3), 262. https://doi.org/10.3390/rs8030262

Beelen, R., Hoek, G., Vienneau, D., Eeftens, M., Dimakopoulou, K., Pedeli, X., et al. (2013). Development of NO_2 and NOx land use regression models for estimating air pollution exposure in 36 study areas in Europe—the ESCAPE project. *Atmospheric Environment*, *72*(2), 10–23. https://doi.org/10.1016/j.atmosenv.2013.02.037

Braggio, J. T., Hall, E. S., Weber, S. A., & Huff, A. K. (2021). Contribution of AOD-PM2.5 surfaces to respiratory-cardiovascular hospital events in urban and rural areas in Baltimore, Maryland, USA: New analytical method correctly identified true positive cases and true negative controls. *Atmospheric Environment*, *262*, 118629. https://doi.org/10.1016/j.atmosenv.2021.118629

Cai, L., Zhuang, M., & Ren, Y. (2020). A landscape scale study in Southeast China investigating the effects of varied green space types on atmospheric PM2.5 in mid-winter. *Urban Forestry and Urban Greening*, *49*, 126607. https://doi.org/10.1016/j.ufug.2020.126607

Chen, C. C., Wang, Y. R., Yeh, H. Y., Lin, T. H., Huang, C. S., & Wu, C. F. (2021). Estimating monthly $PM_{2.5}$ concentrations from satellite remote sensing data, meteorological variables, and land use data using ensemble statistical modeling and a random forest approach. *Environmental Pollution*, *291*, 118159. https://doi.org/10.1016/j.envpol.2021.118159

Chen, W., Ran, H., Cao, X., Wang, J., Teng, D., Chen, J., & Zheng, X. (2020). Estimating $PM_{2.5}$ with high-resolution 1-km AOD data and an improved machine learning model over Shenzhen, China. *Science of the Total Environment*, *746*, 141093. https://doi.org/10.1016/j.scitotenv.2020.141093

Edwards, L., Rutter, G., Iverson, L., Wilson, L., Chadha, T. S., Wilkinson, P., & Milojevic, A. (2021). Personal exposure monitoring of $PM_{2.5}$ among US diplomats in Kathmandu during the COVID-19 lockdown, March to June 2020. *Science of the Total Environment*, *772*, 144836. https://doi.org/10.1016/j.scitotenv.2020.144836

Ghahremanloo, M., Choi, Y., Sayeed, A., Salman, A. K., Pan, S., & Amani, M. (2021). Estimating daily high-resolution $PM_{2.5}$ concentrations over Texas: Machine learning approach. *Atmospheric Environment*, *247*, 118209. https://doi.org/10.1016/j.atmosenv.2021.118209

Gong, F. Y., Zeng, Z. C., Zhang, F., Li, X., Ng, E., & Norford, L. K. (2018). Mapping sky, tree, and building view factors of street canyons in a high-density urban environment. *Building and Environment*, *134*, 155–167. https://doi.org/10.1016/j.buildenv.2018.02.042

Hohenberger, T. L., Che, W., Fung, J. C. H., & Lau, A. K. H. (2021). A proposed population-health based metric for evaluating representativeness of air quality monitoring in cities: Using Hong Kong as a demonstration. *PLoS One*, *16*(5), e0252290. https://doi.org/10.1371/journal.pone.0252290

Hsu, W. T., Chen, J. L., Candice Lung, S. C., & Chen, Y. C. (2020). $PM_{2.5}$ exposure of various microenvironments in a community: Characteristics and applications. *Environmental Pollution*, *263*, 114522. https://doi.org/10.1016/j.envpol.2020.114522

Huang, B., Wu, B., & Barry, M. (2010). Geographically and temporally weighted regression for modeling spatio-temporal variation in house prices. *International Journal of Geographical Information Science*, *24*(3), 383–401. https://doi.org/10.1080/13658810802672469

Jiang, Z., Jolleys, M. D., Fu, T. M., Palmer, P. I., Ma, Y., Tian, H., et al. (2020). Spatiotemporal and probability variations of surface $PM_{2.5}$ over China between 2013 and 2019 and the associated changes in health risks: An integrative observation and model analysis. *Science of the Total Environment*, *723*, 137896. https://doi.org/10.1016/j.scitotenv.2020.137896

Kang, Y., Zhang, F., Gao, S., Lin, H., & Liu, Y. (2020). A review of urban physical environment sensing using street view imagery in public health studies. *Annals of GIS*, *26*(3), 261–275. https://doi.org/10.1080/19475683.2020.1791954

Lee, H. J., Chatfield, R. B., & Strawa, A. W. (2016). Enhancing the applicability of satellite remote sensing for $PM_{2.5}$ estimation using MODIS deep blue AOD and land use regression in California, United States. *Environmental Science & Technology*, *50*(12), 6546–6555. https://doi.org/10.1021/acs.est.6b01438

Li, G., Ren, Z., & Zhan, C. (2020). Sky view factor-based correlation of landscape morphology and the thermal environment of street canyons: A case study of Harbin, China. *Building and Environment*, *169*, 106587. https://doi.org/10.1016/j.buildenv.2019.106587

Li, J., Garshick, E., Hart, J. E., Li, L., Shi, L., Al-Hemoud, A., et al. (2021). Estimation of ambient $PM_{2.5}$ in Iraq and Kuwait from 2001 to 2018 using machine learning and remote sensing. *Environment International*, *151*, 106445. https://doi.org/10.1016/j.envint.2021.106445

Li, J., Zhang, H., Chao, C. Y., Chien, C. H., Wu, C. Y., Luo, C. H., et al. (2020). Integrating low-cost air quality sensor networks with fixed and satellite monitoring systems to study ground-level $PM_{2.5}$. *Atmospheric Environment*, *223*, 117293. https://doi.org/10.1016/j.atmosenv.2020.117293

Li, R., Ma, T., Xu, Q., & Song, X. (2018). Using MAIAC AOD to verify the $PM_{2.5}$ spatial patterns of a land use regression model. *Environmental Pollution*, *243*, 501–509. https://doi.org/10.1016/j.envpol.2018.09.026

Li, T., Shen, H., Zeng, C., & Yuan, Q. (2020). A validation approach considering the uneven distribution of ground stations for satellite-based $PM_{2.5}$ Estimation. *Ieee Journal of Selected Topics in Applied Earth Observations and Remote Sensing*, *13*, 1312–1321. https://doi.org/10.1109/JSTARS.2020.2977668

Li, X., & Feng, Y. (2018). Estimating spatio-temporal variations of $PM_{2.5}$ over Hong Kong using an improved GTWR model and SARA AOD retrievals. *Photogrammetric Engineering & Remote Sensing*, *84*(12), 761–769. https://doi.org/10.14358/PERS.84.12.761

Li, X., Zhang, C., Li, W., Ricard, R., Meng, Q., & Zhang, W. (2015). Assessing street-level urban greenery using Google Street View and a modified green view index. *Urban Forestry and Urban Greening*, *14*(3), 675–685. https://doi.org/10.1016/j.ufug.2015.06.006

Liu, J., Weng, F., & Li, Z. (2019). Satellite-based $PM_{2.5}$ estimation directly from reflectance at the top of the atmosphere using a machine learning algorithm. *Atmospheric Environment*, *208*, 113–122. https://doi.org/10.1016/j.atmosenv.2019.04.002

Liu, Y., Gao, S., Yuan, Y., Zhang, F., Kang, C., Kang, Y., & Wang, K. (2021). Methods of Social sensing for urban studies. *Urban Remote Sensing*, 71–89. https://doi.org/10.1002/9781119625865.ch4

Lu, Y., Giuliano, G., & Habre, R. (2021). Estimating hourly $PM_{2.5}$ concentrations at the neighborhood scale using a low-cost air sensor network: A Los Angeles case study. *Environmental Research*, *195*, 110653. https://doi.org/10.1016/j.envres.2020.110653

Lung, S. C. C., Wang, W. C. V., Wen, T. Y. J., Liu, C. H., & Hu, S. C. (2020). A versatile low-cost sensing device for assessing $PM_{2.5}$ spatiotemporal variation and quantifying source contribution. *Science of the Total Environment*, *716*(128), 137145. https://doi.org/10.1016/j.scitotenv.2020.137145

Meng, X., Liu, C., Zhang, L., Wang, W., Stowell, J., Kan, H., & Liu, Y. (2021). Estimating $PM_{2.5}$ concentrations in Northeastern China with full spatiotemporal coverage, 2005–2016. *Remote Sensing of Environment*, *253*, 112203. https://doi.org/10.1016/j.rse.2020.112203

Mishra, R. K., Agarwal, A., & Shukla, A. (2021). Predicting ground level $PM_{2.5}$ concentration over Delhi using Landsat 8 satellite data. *International Journal of Remote Sensing*, *42*(3), 827–838. https://doi.org/10.1080/2150704X.2020.1832279

Mo, Y., Booker, D., Zhao, S., Tang, J., Jiang, H., Shen, J., et al. (2021). The application of land use regression model to investigate spatiotemporal variations of $PM_{2.5}$ in Guangzhou, China: Implications for the public health benefits of $PM_{2.5}$ reduction. *Science of the Total Environment*, *778*, 146305. https://doi.org/10.1016/j.scitotenv.2021.146305

Nazarenko, Y., Pal, D., & Ariya, P. A. (2021). Air quality standards for the concentration of particulate matter 2.5, global descriptive analysis. *Bulletin of the World Health Organization*, *99*(2), 125–137. https://doi.org/10.2471/BLT.19.245704

Ouzemou, J. E., El Harti, A., Lhissou, R., El Moujahid, A., Bouch, N., El Ouazzani, R., et al. (2018). Crop type mapping from pansharpened Landsat 8 NDVI data: A case of a highly fragmented and intensive agricultural system. *Remote Sensing Applications: Society and Environment*, *11*, 94–103. https://doi.org/10.1016/j.rsase.2018.05.002

Shen, H., Li, T., Yuan, Q., & Zhang, L. (2018). Estimating regional ground-level $PM_{2.5}$ directly from satellite top-of-atmosphere reflectance using deep belief networks. *Journal of Geophysical Research: Atmospheres*, *123*(24), 13–875. https://doi.org/10.1029/2018JD028759

Shi, G., Leung, Y., Zhang, J. S., Fung, T., Du, F., & Zhou, Y. (2021). A novel method for identifying hotspots and forecasting air quality through an adaptive utilization of spatio-temporal information of multiple factors. *Science of the Total Environment*, *759*, 143513. https://doi.org/10.1016/j.scitotenv.2020.143513

Shi, Y., Ho, H. C., Xu, Y., & Ng, E. (2018). Improving satellite aerosol optical Depth-$PM_{2.5}$ correlations using land use regression with microscale geographic predictors in a high-density urban context. *Atmospheric Environment*, *190*, 23–34. https://doi.org/10.1016/j.atmosenv.2018.07.021

Shi, Y., Lau, K. K. L., & Ng, E. (2016). Developing street-level $PM_{2.5}$ and PM_{10} land use regression models in high-density Hong Kong with urban morphological factors. *Environmental Science and Technology*, *50*(15), 8178–8187. https://doi.org/10.1021/acs.est.6b01807

Shogrkhodaei, S. Z., Razavi-Termeh, S. V., & Fathnia, A. (2021). Spatio-temporal modeling of $PM_{2.5}$ risk mapping using three machine learning algorithms. *Environmental Pollution*, *289*, 117859. https://doi.org/10.1016/j.envpol.2021.117859

Su, J. G., Jerrett, M., & Beckerman, B. (2009). A distance-decay variable selection strategy for land use regression modeling of ambient air pollution exposures. *Science of the Total Environment*, *407*(12), 3890–3898. https://doi.org/10.1016/j.scitotenv.2009.01.061

Szczerba, R. J., Galkowski, P., Glickstein, I. S., & Ternullo, N. (2000). Robust algorithm for real-time route planning. *IEEE Transactions on Aerospace and Electronic Systems*, *36*(3), 869–878. https://doi.org/10.1109/7.869506

The University of Hong Kong. (2022). Historical data of health outcomes. Retrieved from http://hedleyindex.hku.hk/historical

Tong, C., Shi, Z., Shi, W., Zhao, P., & Zhang, A. (2021). Mapping microscale $PM_{2.5}$ distribution on walkable roads in a high-density city. *IEEE Journal of Selected Topics in Applied Earth Observations and Remote Sensing*, *14*, 6855–6870. https://doi.org/10.1109/JSTARS.2021.3075442

United Nations. (2020). A handbook on sustainable urban mobility and spatial planning. https://doi.org/10.18356/8d742f54-en

United Nations Environment Programme. (2020). Walkable streets equals clean air. Retrieved from https://www.unep.org/news-and-stories/story/walkable-streets-equals-clean-air

Vienneau, D., DeHoogh, K., Bechle, M. J., Beelen, R., VanDonkelaar, A., Martin, R. V., et al. (2013). Western European land use regression incorporating satellite- and ground-based measurements of NO_2 and PM_{10}. *Environmental Science and Technology*, *47*(23), 13555–13564. https://doi.org/10.1021/es403089q

Wang, Z., Zhou, Y., Zhao, R., Wang, N., Biswas, A., & Shi, Z. (2021). High-resolution prediction of the spatial distribution of $PM_{2.5}$ concentrations in China using a long short-term memory model. *Journal of Cleaner Production*, *297*, 126493. https://doi.org/10.1016/j.jclepro.2021.126493

Wei, J., Li, Z., Lyapustin, A., Sun, L., Peng, Y., Xue, W., et al. (2021). Reconstructing 1-km-resolution high-quality $PM_{2.5}$ data records from 2000 to 2018 in China: Spatiotemporal variations and policy implications. *Remote Sensing of Environment*, *252*, 112136. https://doi.org/10.1016/j.rse.2020.112136

World Health Organization. (2021). New WHO global gir quality guidelines aim to save millions of lives from air pollution. Retrieved from https://www.who.int/news/item/22-09-2021-new-who-global-air-quality-guidelines-aim-to-save-millions-of-lives-from-air-pollution

Wu, J., Luo, K., Wang, Y., & Wang, Z. (2021). Urban road greenbelt configuration: The perspective of $PM_{2.5}$ removal and air quality regulation. *Environment International*, *157*, 106786. https://doi.org/10.1016/j.envint.2021.106786

Xi, Y., Thinh, N. X., & Li, C. (2019). Preliminary comparative assessment of various spectral indices for built-up land derived from Landsat-8 OLI and Sentinel-2A MSI imageries. *European Journal of Remote Sensing*, *52*(1), 240–252. https://doi.org/10.1080/22797254.2019.1584737

Xu, H., Ta, W., Yang, L., Feng, R., He, K., Shen, Z., et al. (2020). Characterizations of $PM_{2.5}$-bound organic compounds and associated potential cancer risks on cooking emissions from dominated types of commercial restaurants in northwestern China. *Chemosphere*, *261*, 127758. https://doi.org/10.1016/j.chemosphere.2020.127758

Xu, X., Zhang, C., & Liang, Y. (2021). Review of satellite-driven statistical models $PM_{2.5}$ concentration estimation with comprehensive information. *Atmospheric Environment*, *256*, 118302. https://doi.org/10.1016/j.atmosenv.2021.118302

Xue, W., Zhang, J., Zhong, C., Ji, D., & Huang, W. (2020). Satellite-derived spatiotemporal $PM_{2.5}$ concentrations and variations from 2006 to 2017 in China. *Science of the Total Environment*, *712*, 134577. https://doi.org/10.1016/j.scitotenv.2019.134577

Yan, X., Zang, Z., Luo, N., Jiang, Y., & Li, Z. (2020). New interpretable deep learning model to monitor real-time $PM_{2.5}$ concentrations from satellite data. *Environment International*, *144*, 106060. https://doi.org/10.1016/j.envint.2020.106060

Yang, L., Xu, H., & Jin, Z. (2019). Estimating ground-level $PM_{2.5}$ over a coastal region of China using satellite AOD and a combined model. *Journal of Cleaner Production*, *227*, 472–482. https://doi.org/10.1016/j.jclepro.2019.04.231

Yang, L., Xu, H., & Yu, S. (2020). Estimating $PM_{2.5}$ concentrations in Yangtze River Delta region of China using random forest model and the top-of-atmosphere reflectance. *Journal of Environmental Management*, *272*, 111061. https://doi.org/10.1016/j.jenvman.2020.111061

Zhang, D., Du, L., Wang, W., Zhu, Q., Bi, J., Scovronick, N., et al. (2021). A machine learning model to estimate ambient $PM_{2.5}$ concentrations in industrialized highveld region of South Africa. *Remote Sensing of Environment*, *266*, 112713. https://doi.org/10.1016/j.rse.2021.112713

Zhang, R., Chen, G., Yin, Z., Zhang, Y., & Ma, K. (2021). Urban greening based on the supply and demand of atmospheric $PM_{2.5}$ removal. *Ecological Indicators*, *126*, 107696. https://doi.org/10.1016/j.ecolind.2021.107696

Zhang, Y., Wang, W., Ma, Y., Wu, L., Xu, W., & Li, J. (2020). Improvement in hourly $PM_{2.5}$ estimations for the Beijing-Tianjin-Hebei region by introducing an aerosol modeling product from MASINGAR. *Environmental Pollution*, *264*, 114691. https://doi.org/10.1016/j.envpol.2020.114691

Zhang, Z., Wang, J., Hart, J. E., Laden, F., Zhao, C., Li, T., et al. (2018). National scale spatiotemporal land-use regression model for $PM_{2.5}$, PM_{10} and NO_2 concentration in China. *Atmospheric Environment*, *192*, 48–54. https://doi.org/10.1016/j.atmosenv.2018.08.046

Zhao, L., Li, T., Przybysz, A., Guan, Y., Ji, P., Ren, B., & Zhu, C. (2021). Effect of urban lake wetlands and neighboring urban greenery on air PM_{10} and $PM_{2.5}$ mitigation. *Building and Environment*, *206*, 108291. https://doi.org/10.1016/j.buildenv.2021.108291